

# Supplementary material for

## Temperature and strain controls on ice deformation mechanisms: insights from the microstructures of samples deformed to progressively higher strains at -10, -20 and -30°C

5 Sheng Fan<sup>1</sup>, Travis Hager<sup>2</sup>, David J. Prior<sup>1</sup>, Andrew J. Cross<sup>2,3</sup>, David L. Goldsby<sup>2</sup>, Chao Qi<sup>4</sup>, Marianne Negrini<sup>1</sup>, John Wheeler<sup>5</sup>

<sup>1</sup> Department of Geology, University of Otago, Dunedin, New Zealand

<sup>2</sup> Department of Earth and Environmental Science, University of Pennsylvania, Philadelphia, PA, USA

<sup>3</sup> Department of Geology and Geophysics, Woods Hole Oceanographic Institution, Woods Hole, MA, USA

10 <sup>4</sup> Institute of Geology and Geophysics, Chinese Academy of Sciences, Beijing, China

<sup>5</sup> Department of Earth and Ocean Sciences, University of Liverpool, Liverpool, UK

### Contents of this file

Text S1 to S2

15 Figure S1

### Introduction

Supplementary material provides the sensitivity test of the co-latitude range (Text S1, Figure S1) in the plot of MUD as a function of co-latitude for the calculation of opening-angle of *c*-axis cone; the mathematical background (Text S2) for the  
20 conversion between engineering strain/strain rate, true axial strain/strain rate and octahedral shear strain/strain rate.

### Text S1 Sensitivity test of the co-latitude range chosen for the plot of MUD as a function co-latitude

In order to quantify cone opening-angles, we counted the number of *c*-axes that lie at a given angle (“co-latitude”) from the compression axis. In practice we counted the *c*-axes between two co-latitudes separated by a co-latitude range and calculated the MUD for this co-latitude range to plot on a graph of MUD as a function of co-latitude. We tested the sensitivity of  
25 co-latitude range for the plot of MUD as a function of co-latitude.

Fig. S1 shows the distribution of MUD as a function of co-latitude with the co-latitude ranges of 2°, 4°, 6° and 8° for three different examples, including PIL165 (with random CPO), PIL177 (with cone-shaped *c*-axis CPO) and PIL166 (with narrow-cone-shaped *c*-axis CPO). The MUD distribution as a function of co-latitude is generally consistent for different co-latitude ranges. However, the MUD value for *c*-axes that lie within ~2° to the centre of the stereonet is sensitive to the value  
30 of co-latitude range. For sample PIL177, which is characterised by a cone-shaped *c*-axis CPO, there is a peak at ~2° in the MUD distribution with the co-latitude range of 2°. This peak cannot be recognized from the contoured *c*-axis CPO.

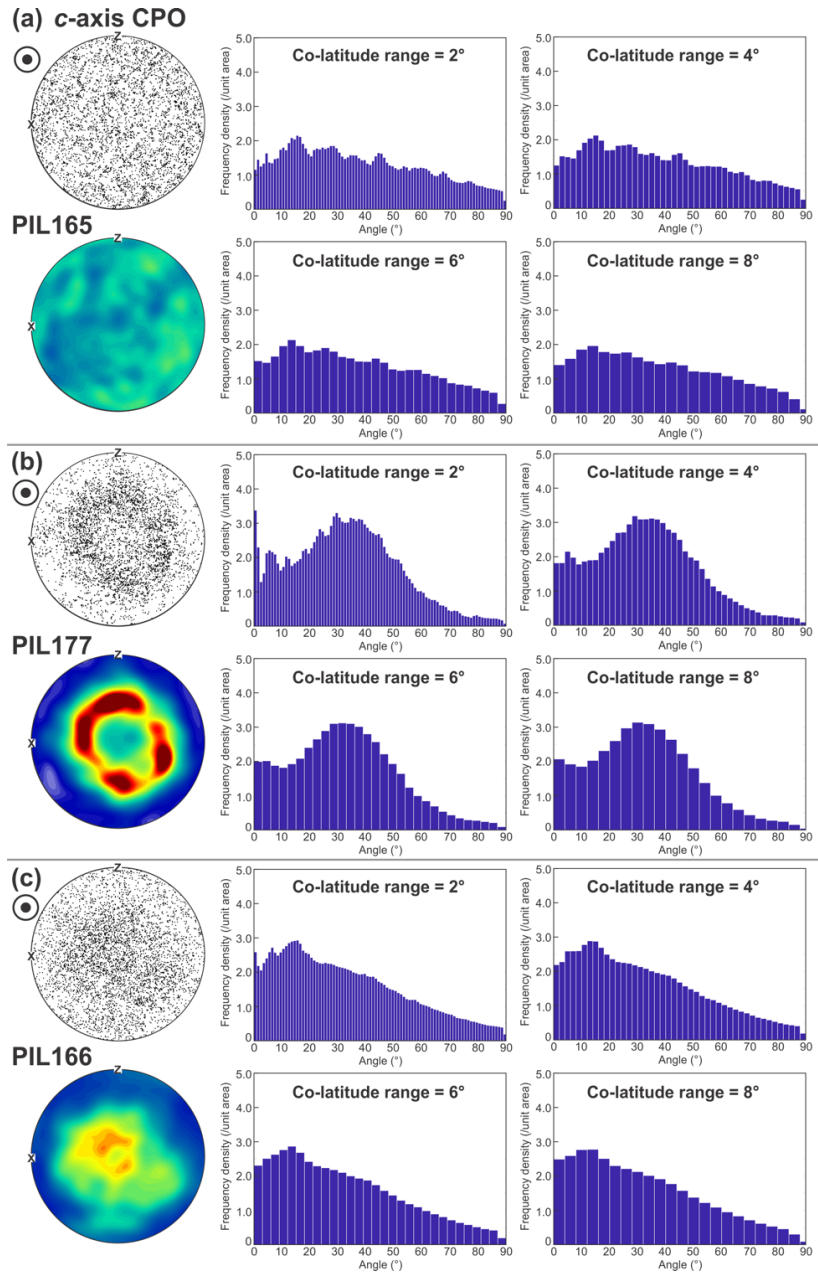


**Figure S1.** Sensitivity test of co-latitude range on samples of **(a)** PIL 165, characterised by a random CPO, **(b)** PIL177, characterised by a cone-shaped *c*-axis CPO and **(c)** PIL166, characterised by a narrow-cone-shaped *c*-axis CPO. For each sample, the upper left box is the point pole figure with 5000 randomly selected points and the lower left box is the corresponding contoured *c*-axis CPO. The centre of the stereonet is parallel to compression. The right part contains MUD distribution as a function of co-latitude with the co-latitude ranges of 2°, 4°, 6° and 8°.

## Text S2 Mechanical data processing

The raw data of the axial displacement readings as a function of time were processed to obtain strain and strain rate. Engineering axial strain  $e$ , true axial strain  $\varepsilon$  and octahedral shear strain  $\gamma$  are most frequently used parameters to quantify the sample deformation in published literatures. In this study,  $\varepsilon$  and  $\gamma$  were converted to  $e$  for a direct comparison of the data  
5 from this study and literatures.

In an uniaxial compression experiment, we define the axial stretch  $\lambda$  (Eq. (S1)) as the ratio of the sample length  $(L(t))$  at time  $t$  and the initial sample length  $(L_0)$ .

$$\lambda = \frac{L(t)}{L_0} \quad (\text{Equation S1})$$

The true axial strain  $\varepsilon$ , at time  $t$ , is given by:

$$\begin{aligned} \varepsilon &= -\ln\left(\frac{L(t)}{L_0}\right) \\ &= -\ln(\lambda) \end{aligned} \quad (\text{Equation S2})$$

The engineering axial strain  $e$  at time  $t$  is given by:

$$\begin{aligned} e &= \frac{L_0 - L(t)}{L_0} \\ &= 1 - \lambda \end{aligned} \quad (\text{Equation S3})$$

15 Therefore, the conversion between true axial strain  $\varepsilon$  and engineering axial strain  $e$  can be expressed as:

$$\varepsilon = -\ln(1 - e) \quad (\text{Equation S4})$$

The octahedral shear strain  $\gamma$  at time  $t$  is given by:

$$\gamma = \frac{1}{3} \sqrt{(\varepsilon_1 - \varepsilon_2)^2 + (\varepsilon_2 - \varepsilon_3)^2 + (\varepsilon_3 - \varepsilon_1)^2}, \quad (\text{Equation S5})$$

where  $\varepsilon_1$ ,  $\varepsilon_2$  and  $\varepsilon_3$  represent principle engineering strains. For uniaxial compression, we suppose the horizontal shortening  
20 is radially uniform ( $\varepsilon_2 = \varepsilon_3$ ). Therefore, Eq. (S5) can be simplified as:

$$\gamma = \frac{\sqrt{2}}{3} (\varepsilon_1 - \varepsilon_3), \quad (\text{Equation S6})$$

where the principle axial engineering strain  $\varepsilon_1$  equals to  $e$ . We suppose the sample volume remains unchanged during uniaxial compression. The sample volume  $V$  is given by:

$$\begin{aligned} V &= \pi R_0^2 L_0 \\ &= \pi R(t)^2 L(t), \end{aligned} \quad (\text{Equation S7})$$

where  $R_0$  is the initial sample radius,  $R(t)$  is the sample radius at time  $t$ . Therefore,  $R(t)$  is given by:

$$R(t) = R_0 \sqrt{\frac{L_0}{L(t)}}$$

$$= R_0 \frac{1}{\sqrt{\lambda}} \quad (\text{Equation S8})$$

The principle radius engineering strain  $\epsilon_3$  is given by:

$$\begin{aligned} \epsilon_3 &= \frac{R_0 - R(t)}{R_0} \\ &= 1 - \frac{R(t)}{R_0} \\ &= 1 - \frac{1}{\sqrt{\lambda}} \\ &= 1 - \frac{1}{\sqrt{1-e}} \end{aligned} \quad (\text{Equation S9})$$

Therefore, Eq. (S6) can be converted to:

$$\gamma = \frac{\sqrt{2}}{3} \left( e + \frac{1}{\sqrt{1-e}} - 1 \right) \quad (\text{Equation S10})$$

In this study, the axial displacement remains constant, but the sample length keeps decreasing with time. Consequently, the axial strain rate increases with time. The engineering axial strain rate ( $\dot{e}$ ) is given by:

$$\dot{e} = \frac{d(e)}{dt} \quad (\text{Equation S11})$$

The relationship between true axial strain rate ( $\dot{\epsilon}$ ) and engineering axial strain rate ( $\dot{e}$ ) is given by:

$$\begin{aligned} \dot{\epsilon} &= \frac{d(\epsilon)}{dt} \\ &= -\frac{d}{dt} (\ln(1-e)) \\ &= \frac{1}{1-e} \frac{d(e)}{dt} \\ &= \frac{\dot{e}}{1-e} \end{aligned} \quad (\text{Equation S12})$$

The relationship between octahedral shear strain rate ( $\dot{\gamma}$ ) and engineering axial strain rate ( $\dot{e}$ ) is given by:

$$\begin{aligned} \dot{\gamma} &= \frac{d(\gamma)}{dt} \\ &= \frac{\sqrt{2}}{3} \frac{d}{dt} \left( e + \frac{1}{\sqrt{1-e}} - 1 \right) \\ &= \frac{\sqrt{2}}{3} \left( \frac{d(e)}{dt} + \frac{d}{dt} \left( \frac{1}{\sqrt{1-e}} \right) \right) \\ &= \frac{\sqrt{2}}{3} \left( 1 + \frac{1}{2(1-e)^{\frac{3}{2}}} \right) \frac{d(e)}{dt} \end{aligned}$$

$$= \frac{\sqrt{2}}{3} \left( 1 + \frac{1}{2(1-e)^{\frac{3}{2}}} \right) e$$

(Equation S13)